Journal of Medicinal Chemistry

Article

Charge Dependence of Cellular Uptake and Selective Antitumor Activity of Porphyrazines

Neal D. Hammer, Sangwan Lee, Benjamin J. Vesper, Kim M. Elseth, Brian M. Hoffman, Anthony G. M. Barrett, and James A. Radosevich

J. Med. Chem., **2005**, 48 (26), 8125-8133• DOI: 10.1021/jm050466y • Publication Date (Web): 12 November 2005

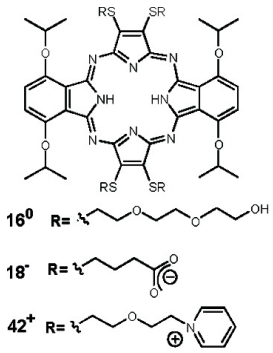

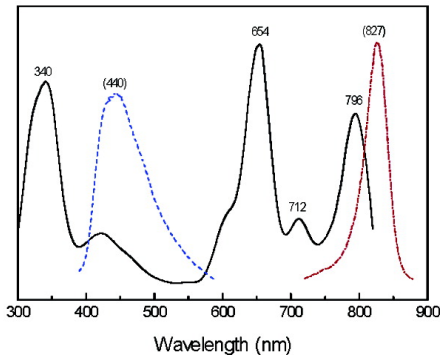

More About This Article

Additional resources and features associated with this article are available within the HTML version:

- Supporting Information
- Links to the 4 articles that cite this article, as of the time of this article download
- Access to high resolution figures
- Links to articles and content related to this article
- Copyright permission to reproduce figures and/or text from this article

View the Full Text HTML

Journal of Medicinal Chemistry is published by the American Chemical Society. 1155 Sixteenth Street N.W., Washington, DC 20036

Charge Dependence of Cellular Uptake and Selective Antitumor Activity of Porphyrazines

Neal D. Hammer,[†,‡] Sangwan Lee,[§] Benjamin J. Vesper,[§] Kim M. Elseth,[†,‡] Brian M. Hoffman,[§] Anthony G. M. Barrett,[||] and James A. Radosevich*[,†,‡]

Center for Molecular Biology of Oral Diseases, University of Illinois—Chicago, Chicago, Illinois 60612, Department of Chemistry, Northwestern University, Evanston, Illinois 60208, Jesse Brown VA Medical Center, Chicago, Illinois 60612, and Department of Chemistry, Imperial College of Science, Technology and Medicine, South Kensington, London, SW7 2AZ, UK

Received May 17, 2005

Porphyrazines (pzs), or tetraazaporphyrins, can be viewed as porphyrinic macrocycles in which the porphyrin meso (CH) groups are replaced by nitrogen atoms; as such, it can be anticipated that pzs would show similar biocompatibility and biodistribution to those of porphyrins. However, distinctive chemical and physical features of the pzs differentiate them from either the porphyrins or phthalocyanines, in particular making them excellent candidates as optical imaging/therapeutic agents. The novelty of the pzs requires that we first determine how specific structures selectively alter biological function, leading to the development of "rules" that will be used to predict future biologically functional pzs. In the first of these studies, we present here a correlation of pz charge with biocompatibility for a suite of three pzs—neutral, negative, and positive. Confocal fluorescence microscopy and proliferation/viability measurements disclose that the three pzs differ in their toxicity, uptake, and localization in A549 human lung adenocarcinoma cells and WI-38 VA13 normal cells. Interestingly, the negatively charged pz exhibits selective dark toxicity in pulmonary adenocarcinoma cells.

Introduction

The use of porphyrins as biomedical agents has been widely explored, with the most notable event being the first clinical use of a porphyrin, Photofrin (hematoporphyrin derivative, HpD), as a photodynamic therapy (PDT) agent.[1−4] The utility of a compound as an optical agent, both in PDT and in the complementary role as contrast agent for optical absorbance/fluorescence imaging of soft tissue,[5−8] depends on the fact that mammalian tissue absorbs near-infrared (NIR) light only weakly at wavelengths beyond the absorbance of hemoglobin, $\lambda \leq 700$ nm, and below the onset of absorbance by water, $\lambda \geq 900$ nm.[9−11] If a dye with high molar absorptivity in this window preferentially accumulates in tumors and exhibits a high quantum yield for the generation of singlet oxygen, it is of potential use in PDT applications.[3,4] On the other hand, if it preferentially accumulates, has high molar absorptivity *and* strong fluorescence, preferably with poor singlet oxygen sensitization, it has potential as a contrast agent in optical imaging of tumors in soft tissue.[5−8] Porphyrins exhibit selective uptake by tumors, but they meet the optical criteria rather poorly.[12] As a result, interest has shifted to the use of what may be viewed as porphyrin "variants": phthalocyanines, which have superior optical properties but intrinsic limitations in solubility;[13,14] benzoporphyrins;[15] chlorins and bacteriochlorins;[16] and expanded porphyrins.[17] We report here the first examination of the biological properties of a long-known but relatively unstudied class of macrocycles, the porphyrazines (pzs), which have excellent optical properties.[18]

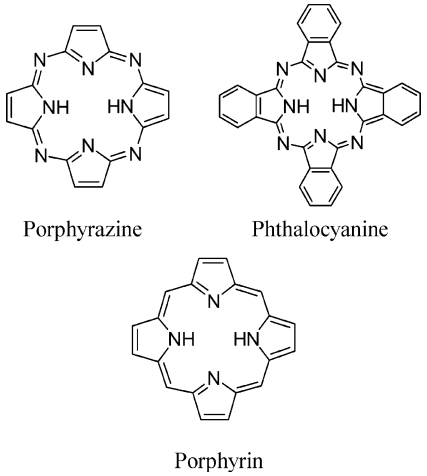

Figure 1. Structural differences among porphyrins, phthalocyanines, and porphyrazines.

Porphyrazines (pzs), or tetraazaporphyrins, can be viewed as porphyrinic macrocycles in which the porphyrin meso (CH) groups are replaced by nitrogen atoms linking the pyrrole rings (Figure 1); with this degree of similarity, they can be anticipated to show similar biocompatibility and biodistribution to those of porphyrins. However, distinctive chemical and physical features of the pzs differentiate them from either the porphyrins or phthalocyanines.[18] (i) The *meso*-nitrogens of the pzs confer on them intense long-wavelength absorbance and emission bands, photophysical properties that are intrinsically superior to those of the

* Corresponding author. Phone (312) 996-9538. Fax: (312) 996-9592. E-mail: jrados@uic.edu.
† University of Illinois—Chicago.
‡ Jesse Brown VA Medical Center.
§ Northwestern University.
|| Imperial College of Science, Technology and Medicine.

10.1021/jm050466y CCC: $30.25
Published on Web 11/12/2005

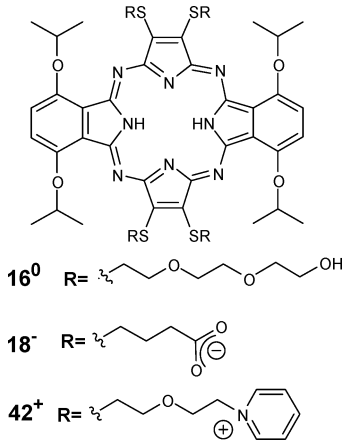

Figure 2. The three porphyrazines subjected to biological assays in this study.

porphyrins. Indeed, with nothing more than simple carbon-based substituents, the photophysical properties of pzs are comparably favorable to those of the phthalocyanines, and these can be improved with proper derivatization. (ii) Although porphyrins and pzs have similar structures, they are synthesized by entirely different routes: pzs by the template cyclization of maleonitrile derivatives and porphyrins by the condensation of pyrrole and aldehyde derivatives. As a result, pzs can be readily prepared with S, N, or O heteroatoms attached to the macrocycle core,[19−26] but porphyrins cannot. Such heteroatom substituents can help to tune the photophysical properties of pzs so that they exhibit optimal NIR absorbance and emission within the 700−900 nm window, as well as also to tune their singlet oxygen quantum yields from essentially *off* to *on*.[27]

We here present the first detailed study of the biological influences of the porphyrazines, aimed at developing structure−function correlations that will be used to predict future biologically active porphyrazines. Given that both positively and negatively charged porphyrins and phthalocyanines have shown promise as PDT photosensitizers,[14,28−30] we chose to begin the porphyrazine structure−function studies by analyzing a trio of pzs varying in charge—neutral (**16**^{0}), negative (**18**$^-$), and positive (**42**$^+$) (Figure 2). (To aid the reader, the superscript denotes the overall charge of the pzs in biological media as being neutral, negatively, or positively charged, respectively.) Each of the three pzs consists of two $[S-R]_2$ units substituted on one pair of opposing pyrroles of the macrocycle core and two β,β'-dialkoxybenzo groups are fused to the other pair of opposing pyrroles. Compounds of this pz subclass display intense UV and near-IR absorbance and dual UV−visible/near-IR emission; by changing the R group, one can change the solubility and/or charge of the compound while leaving the photophysical properties unchanged,[31,32] characteristics that make the pzs excellent candidates as optical biomedical agents. We present confocal fluorescence microscopic visualization of cellular uptake and localization, concentration/time-dependent cytotoxicity measurements, and phototoxicity measurements for **16**^{0}, **18**$^-$, and **42**$^+$ in A549 tumor and WI-38 VA13 normal cells. Interestingly, **18**$^-$ exhibits selective dark toxicity in pulmonary adenocarcinoma cells.

Experimental Section

Abbreviations: HpD, hematoporphyrin derivative; NIR, near-infrared; PDT, photodynamic therapy; pz(s), porphyrazine(s).

Chemicals and Instrumentation. All chemicals were purchased from Aldrich Chemical Co. and used without further purification. Silica gel used for chromatography was Baxter silica gel (60 Å, 230−400 mesh). Electronic absorption spectra were recorded on a Hewlett-Packard HP8452A diode-array spectrophotometer and a Varian Cary 1E UV−visible spectrometer. Electronic emission spectra were recorded using a Photon Technology International QM2 fluorescence spectrometer. ^{1}H NMR spectra were obtained using a Mercury 300 MHz spectrometer. Electrospray ionization mass spectra (ESI-MS) were recorded using a Finnigan LCQ Advantage or Micromass Quatro II Electronic HPLC−MS/MS mass spectrometer.

Porphyrazine Synthesis. Disodium 1,2-dicyano-1,2-ethenedithiolate (Na_2MNT),[33] bis{2-[2-(2-hydroxyethoxy)ethoxy]ethylthio}maleonitrile ($MNT[(C_2H_4O)_3H]_2$, **2**),[31] dimethyl-6,7-dicyano-5,8-dithia-6(*Z*)-dodecenedioate ($MNT(C_4O_2Me)_2$, **3**),[32] 1-imino-4,7-bis(1-methylethoxy)-1*H*-isoindolin-3-amine (diiminoisoindoline, **4**),[32] and pzs **16**,[31] **17**,[32] and **18**[32] were prepared as previously reported. Each pz was prepared as a 5 mM working stock solution in DMSO for use in the tissue culture experiments.

Bis[2-(2-hydroxyethoxy)ethylthio]maleonitrile (1). To a suspension of Na_2MNT (18.6 g, 0.1 mol) in acetone (300 mL) were added 2-(2-chloroethoxy)ethanol (24.92 g, 0.2 mol) and NaI (ca. 3 g). The reaction was stirred at reflux under a nitrogen atmosphere for 1 day. The solvent was then removed under reduced pressure. The residue was dissolved in CH_2Cl_2 and filtered to remove NaCl, NaI, and unreacted Na_2MNT. The resulting residue was chromatographed on silica gel (5% MeOH in CH_2Cl_2 eluant) to provide the title compound (**1**) (17.5 g, 55%) as a viscous yellow oil: ^{1}H NMR (300 MHz, $CDCl_3$) δ 2.57 (br s, 2H, O*H*), 3.35 (t, J = 5.7 Hz, 4H, CH_2CH_2OH), 3.61 (t, J = 3.9 Hz, 4H, CH_2CH_2OH), 3.73−3.80 (m, 8H, SCH_2CH_2O); ESI-MS (*m/z*) $[M + H]^+$ calculated for $C_{12}H_{19}N_2O_4S_2$ 319.07, found 319; $[M + Na]^+$ calculated for $C_{12}H_{18}N_2NaO_4S_2$ 341.06, found 341.

1,4,13,16-Tetrakis(1-methylethoxy)-8,9,20,21-tetrakis-[2-(2-hydroxyethoxy)ethylthio]-*25H,27H*-dibenzo[*b,l*]porphyrazine (15^0). Mg turnings (0.3 g, 12.3 mmol) and I_2 (0.03 g) in *n*-PrOH (180 mL) were heated at reflux for 24 h under N_2 to prepare $Mg(OPr)_2$. $MNT[(C_2H_4O)_2H]_2$ (**1**) (1.60 g, 5.0 mmol) and diiminoisoindoline (**4**) (2.61 g, 10.0 mmol) were added, and the suspension was heated at reflux for 7 h. The solution immediately turned a dark brown color and finally to green-black. The solvent was distilled off under reduced pressure and the green-black residue was dissolved in CH_2Cl_2 (50 mL). TFA (3 mL) was slowly added to the green-black solution, and the solution was stirred at room temperature for 1 h. After dilution with CH_2Cl_2 (100 mL), the mixture was washed with water (~500 mL) to remove TFA and other water-soluble materials, dried (Na_2SO_4), and rotary evaporated. The resulting residue was chromatographed on silica gel (5% MeOH in CH_2Cl_2 eluant) to provide the title porphyrazine (**15**^{0}) (450 mg, 8%) as a dark green solid: UV−vis (CH_2Cl_2) λ_{max} (log ϵ) 340 (4.68), 422 (1.96), 654 (5.40), 712 (2.20), 798 (4.38) nm; ^{1}H NMR (300 MHz, $CDCl_3$) δ −0.57 (br s, 2H, N*H*), 1.81 (d, J = 6.1 Hz, 24 H, $CH(CH_3)_2$), 2.90 (br s, 4H, O*H*), 3.50 (t, J = 4.2 Hz, 8H, CH_2CH_2OH), 3.58 (t, J = 4.2 Hz, 8H, CH_2CH_2OH), 3.83 (t, J = 6.1 Hz, 8H, SCH_2CH_2O), 4.38 (t, J = 6.2 Hz, 8H, SCH_2CH_2O), 5.27 (hp, J = 6.1 Hz, 4H, $CHMe_2$), 7.58 (s, 4H, Ar*H*); ESI-MS (*m/z*) $[M + H]^+$ calculated for $C_{52}H_{71}N_8O_{12}S_4$ 1127.40, found 1127.

1,4,13,16-Tetrakis(1-methylethoxy)-8,9,20,21-tetrakis-[2-(4-methylbenzenesulfonato)ethylthio]-*25H,27H*-dibenzo[*b,l*]porphyrazine (41^0). **15**^{0} (112.8 mg, 0.1 mmol) and TsCl (382 mg, 2 mmol) were dissolved in 2 mL of CH_2Cl_2 in a flask, and triethylamine (61 mg, 0.6 mmol) was added with stirring. After stirring at room temperature for 24 h, the reaction mixture was diluted with CH_2Cl_2 and washed with a large amount of water to remove water-soluble materials. The

organic phase was separated, dried (Na_2SO_4), and rotary evaporated. Chromatography of the resultant solid on silica gel (1.5% MeOH in CH_2Cl_2 eluant) gave the title compound (**41**^{0}) (141 mg, 81%) as a dark green solid: UV−vis (CH_2Cl_2) λ_{max} (log ϵ) 340 (4.80), 422 (1.96), 654 (5.49), 712 (2.22), 798 (4.18) nm; ESI-MS (*m/z*) $[M + H]^+$ calculated for $C_{80}H_{95}N_8O_{20}S_8$ 1743.44, found 1743.

1,4,13,16-Tetrakis(1-methylethoxy)-8,9,20,21-tetrakis-[[2-(2-pyridinioethoxy)ethoxy]ethylthio]-*25H,27H*-dibenzo[*b,l*]porphyrazine (42$^+$). **41**^{0} (34.9 mg, 0.02 mmol) was dissolved in 5 mL of pyridine in a flask and heated at reflux (115 °C) for 10 h with stirring under N_2. After the reaction was completed, the pyridine was evaporated under reduced pressure. Chromatography of the resultant solid on Sephadex LH-20 gel filtration (MeOH eluent) gave the title compound (**42**$^+$) (38.7 mg, 94%) as a dark green solid: UV−vis (CH_2Cl_2) λ_{max} (log ϵ) 340 (5.07), 420 (2.20), 652 (5.49), 710 (2.57), 796 (4.00) nm; ESI-MS (*m/z*) $[M]^{4+}$ calculated for $C_{72}H_{86}N_{12}O_8S_4^{4+}$ 343.64, found 344.0. Anal. Calcd for ($C_{72}H_{86}N_{12}O_8S_4$·$6H_2O$): C, 55.38; H, 5.86; N, 7.75. Found: C, 55.18; H, 5.33; N, 7.27.

Cell Culture. A549, a human lung adenocarcinoma cell line, and WI-38 VA13, a SV40 transfected embryonic cell line, were obtained from ATCC. The A549 cell line was maintained in RPMI 1640 media supplemented with 10% fetal calf serum heat inactivated at 56°C for 30 min, 2 mM L-glutamine, 100 μg/mL streptomycin, 100 U/mL penicillin, and 2.5 μg/mL amphotericin B solution. The WI-38 VA13 cell line was maintained in minimum essential medium (MEM) with Earle's salts supplemented with 10% fetal calf serum heat inactivated at 56°C for 30 min, 2 mM l-glutamine, 100 μg/mL streptomycin, 100 U/mL penicillin, and 2.5 μg/mL amphotericin B solution, as well as 100 μM MEM nonessential amino acids and 1 mM sodium pyruvate solution. Cells were grown at 37 °C in a humidified atmosphere containing 5% CO_2.

With the exception of the amphotericin B solution (Biologos) and sodium pyruvate solution (Cellgro), all media and supplements were purchased from Gibco. DMSO and 3-[4,5-dimethylthiazol-2-yl]-2,5-diphenyltetrazolium bromide (MTT) were purchased from Aldrich Chemical Co. The MTT/PBS solution was sterile filtered (0.2 μm pore size) prior to use. MitoTracker Green and LysoTracker Green were purchased from Molecular Probes. Hematoporphyrin derivative (Photofrin) was obtained from QLT Phototherapeutics, Inc.

Imaging Assays. A549 and WI-38 VA13 cells were plated onto sterilized glass coverslips in 60 × 15 mm dishes and grown at 37 °C in a humidified atmosphere containing 5% CO_2. When the cells were 60−80% confluent, they were treated with pzs at concentrations of 50, 25, 12.5, 6.2, and 3.1 μM and were incubated in the dark under the same conditions for an additional 24 h. In the case of **16**^{0} and **18**$^-$, microscopic examination of the resulting cell preparations disclosed that some of the pz precipitated during incubation. Therefore, the actual dosages are in some cases less than the treatment concentrations added to each test well. Negative controls were prepared by treating cells with an amount of DMSO equivalent to that of the 50 μM pz sample; positive controls employed 50 μM HpD.[34]

Confocal microscopic images of both the blue and red pz emission were obtained at room temperature with a Zeiss 510 LSM confocal microscope. Following the 24 h period for incubation of cells with a pz, the supernatant was decanted and cells were washed twice with PBS. The washed coverslips were then inverted onto microscope slides, and the cells were imaged live in PBS. To measure the UV (S_2) emission, a titanium−sapphire laser was tuned to 700 nm, and the resulting two-photon excitation at 350 nm produced the blue emission, which was detected using a 435−485 nm band-pass filter. It was not possible to monitor red pz emission generated by the two-photon excitation because of interference from the 700-nm laser line. To measure the red (S_1) emission, single-photon excitation with an argon-ion laser line at 488 nm was used, and fluorescence was detected with a long-pass 505-nm filter. Background autofluorescence was removed from control samples by adjusting the detector gain and amplitude controls; samples treated with the pz compounds were then imaged under the same settings.

Intracellular Localization. To determine pz intracellular localization, mitochondrial- and lysosomal-specific dyes were treated concurrently with **16**^{0} in A549 cells. Cells were grown on coverslips in the presence of 100 μM **16**^{0} for 24 h as described above. Following incubation, the pz-containing media was decanted and replaced with fresh media containing either MitoTracker Green (25 nM) or LysoTracker Green (50 nM), and cells were incubated at 37 °C for an additional 45 min. The coverslips were then washed and mounted onto slides as described above. Fluorescence of **16**^{0} was monitored using two-photon excitation as described above; the MitoTracker Green and LysoTracker Green dyes were excited at 488 nm using the argon ion laser, and emission was detected using a 500−550-nm band-pass filter. Since 488-nm excitation of **16**^{0} also generates 500−550-nm emission, **16**^{0} was used as a control for the MitoTracker and LysoTracker dyes: the detector gain and amplitude controls were decreased until fluorescence was no longer observed for 100 μM **16**^{0}; the MitoTracker and LysoTracker samples were then imaged using these adjusted settings.

Cytotoxicity Assays. MTT proliferation/viability assays were used to assess the cytotoxic effect of the pzs**.** Cells were seeded into 96-well microtiter plates and grown until they were 70% confluent. The plates were then treated in the dark (to avoid photosensitized killing) with 100, 50, 25, 12.5, 6.2, 3.1, 1.5 μM porphyrazine, 50 μM HpD, or a volume of DMSO equivalent to the volume of compound added at 100 and 50 μM and incubated for up to 72 h; no decrease in cell viability was observed in either cell line over the 72 h treatment with DMSO. Media was decanted at designated time points, and 200 μg of MTT/PBS in solution was added to each well. The microtiter well plate was incubated at 37 °C in a humidified atmosphere containing 5% CO_2 for 5 h. After the incubation period, the supernatant was decanted and 100 μL of DMSO was added to each well. The absorbance at 540 nm was read for each well. Each data point represents the average of four microtiter well plates for each experiment, and each experiment was conducted at least three times. Values between each experiment were normalized and averaged such that there was a minimum of 12 independent values for each reported condition, for each cell line.

Phototoxicity Assays. Cells were seeded into 96-well plates and incubated with 50 μM pz for 24 h, as described above. After the incubation period, the microtiter plates were placed on top of a standard X-ray illuminator (consisting of four 15-W bulbs, ~3600 lumens total) and exposed to 0, 5, and 10 min of light. Plates were then placed back in the humidified atmosphere for 24 h, after which time an MTT assay was performed to assess cytotoxicity.

Results and Discussion

Pz Synthesis and Properties. The three compounds subjected to biological analysis—**16**^{0}, **18**$^-$, and **42**$^+$ (Figure 2)—exhibit the same basic pz structure, with 1,4-dipropoxybenzo-groups fused trans to the pz core and with two trans pairs of peripherally attached thioether groups. All three compounds were prepared via a magnesium-templated cyclization in which the appropriate maleonitrile precursor was reacted with 1,3-diiminoisoindoline (**4**) as shown in Scheme 1. The neutral pz **16**^{0} was prepared directly by reacting MNT-$[(C_2H_4O)_3)H]_2$ (**2**) and **4** in a 2:3 stoichiometric ratio, followed by demetalation with trifluoroacetic acid.[31] Cyclization of MNT$(C_4O_2Me)_2$ (**3**) and **4** in a 1:6 ratio, followed by demetalation, led to the propyl ester-functionalized pz **17**^{0} in 7% yield. During cyclization in *n*-propanol, the methyl ester was converted to the *n*-propyl ester by transesterification. Hydrolysis of **17**^{0} using an excess of lithium hydroxide in THF/H_2O

Scheme 1. Synthetic Route to Porphyrazines $\mathbf{16}^0$, $\mathbf{18}^-$, and $\mathbf{42}^+$ [a]

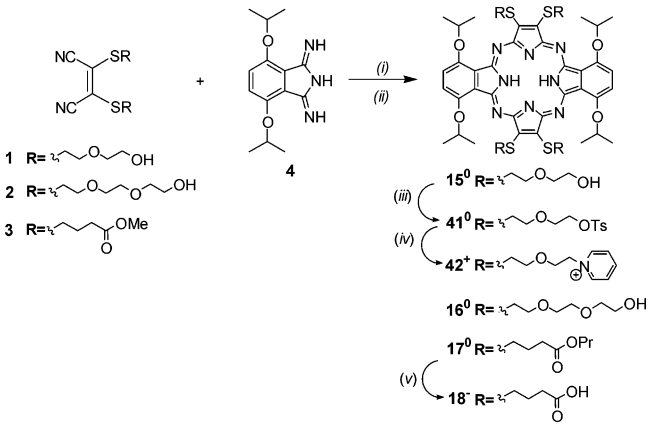

[a] Key: (i) $Mg(OPr)_2$, *n*-PrOH at reflux, 7 h; (ii) TFA, CH_2Cl_2, 20 °C, 1 h; (iii) TsCl, Et_3N, CH_2Cl_2, 24 h; (iv) pyridine at reflux, 10 h; (v) LiOH, THF/H_2O, 20 °C, 4-5 days.

afforded the carboxylic acid $\mathbf{18}^-$ in quantitative yield.[32] The positively charged $\mathbf{42}^+$ was prepared from a pz analogue of $\mathbf{16}^0$: cyclization of $MNT[(C_2H_4O)_2)H]_2$ (**1**) and **4** in a 1:2 ratio, followed by demetalation in trifluoroacetic acid, yielded the neutral pz $\mathbf{15}^0$ in 8% yield; reaction of $\mathbf{15}^0$ with TsCl resulted in the tosylated $\mathbf{41}^0$ at 81%, and subsequent reaction in pyridine gave the target compound $\mathbf{42}^+$ in 94% yield.

The R groups that form the thioethers (Figure 2) do not influence the optical properties; variations in R modulate only the physical properties and solubilities of the parent. Thus, when dissolved in CH_2Cl_2, all three chosen pzs exhibit the same intrinsic absorbance and emission spectra (Figure 3). The absorbance spectrum exhibits a Soret band at 340 nm and split Q-band at 654 and 796 nm, all with high molar absorptivities ($\sim$50 000 M^{-1} cm^{-1}).[18,31,32] This pz subclass exhibits an intense luminescence in the blue, at 440 nm,[27] corresponding to $S_2 \rightarrow$ ground (G) fluorescence, and a second emission in the NIR, at 830 nm, corresponding to $S_1 \rightarrow$ G fluorescence. Excitation to the blue of $\sim$400 nm elicits both the S_1 and S_2 emissions; excitation to the red of $\sim$450 nm produces just the S_1 NIR luminescence.

Because of their different solubilizing side chains, R, the three compounds $\mathbf{16}^0$, $\mathbf{18}^-$, and $\mathbf{42}^+$ have different

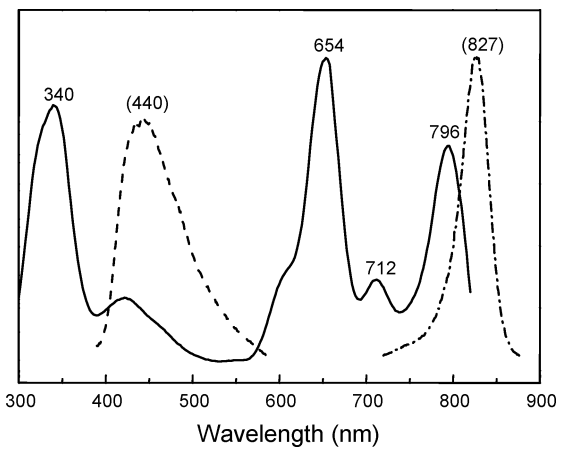

Figure 3. Optical absorption/emission spectra of an $H_2A_2B_2$ pz in CH_2Cl_2. Solid line, absorbance; dashed line, luminescence (normalized).

charges at neutral pH and different solubilities. Compound $\mathbf{16}^0$ is freely soluble in CH_2Cl_2 and DMSO, but not soluble in H_2O; compound $\mathbf{18}^-$ is sparingly soluble in CH_2Cl_2, but is soluble as the acid in DMSO and in basic aqueous solutions, pH $\geq$7.4; $\mathbf{42}^+$ is soluble both in organic solvents and H_2O. Since all three are sufficiently soluble in DMSO, this water-miscible, biologically compatible solvent was used in preparing stock solutions for the various biological assays.

While all three agents show the same intrinsic optical properties when dissolved in CH_2Cl_2, of the three, only $\mathbf{42}^+$ maintains a similar absorbance/emission spectrum when dissolved in DMSO. Although $\mathbf{16}^0$ and $\mathbf{18}^-$ form visibly homogeneous DMSO solutions, the molecules nonetheless undergo intermolecular interactions between the pzs, which broaden the B-bands and quench the NIR fluorescence. Such aggregation phenomena, however, do not quench the UV emission.

Previous studies of pzs of the form $M[pz(A_n;B_{4-n})]$, where A is $[S-R]_2$ and B is a fused β,β'-dialkoxybenzo group, have shown that the singlet oxygen quantum yields (Φ_Δ) of these compounds are dependent upon *M* and *n* but independent of R. The Φ_Δ values can therefore be "tuned" from high to low, making pzs applicable as either therapeutic *or* imaging agents. Each of the three pzs examined in this study are of the form $H_2[pz(A_2;B_2)]$ and thus possess the same quantum yield, $\Phi_\Delta = 0.13$.

Biological Compatibility/Cell Uptake. Initial experiments were undertaken to assess the biological compatibility of the pzs with both A549 human lung adenocarcinoma and WI-38 VA13 normal cell lines. The A549 is a well-established human cell line that has been extensively characterized.[35,36] WI-38 VA13 is derived from a human fibroblast-like cell line of embryonic origin (WI-38), which has been immortalized via SV40 tranfection.[37,38] WI-38 will senesce and is sensitive to passage number with regard to its biological properties.[39] While WI-38 is closer to being a truly "normal" cell, we chose to use WI-38 VA13 because of its consistency in biological properties irrespective of passage number. In pilot studies (data not shown) we found no differences between low passage WI-38 and WI-38 VA13 in the proliferation/viability studies employed herein. High passage number WI-38 cultures resulted in greater variability in proliferation/viability assays due to greater differences in growth rates. We therefore opted to use WI-38 VA13 as a more consistent "tool" to compare to A549, which is also passage insensitive.[35]

Cells were exposed to various concentrations of pz and visually observed for growth, cell morphological changes, and fluorescence in 24-well multicluster plates over a 72 h period. These experiments showed that there was (1) no gross toxicity due to the pzs or the DMSO (data not shown), (2) notable growth (data not shown), (3) no change in cellular morphology, and (4) fluorescence from intracellular pzs that varied with the cell type and pz used (Figures 4 and 5).

Figure 4 presents the confocal microscopic images of A549 and WI-38 VA13 cells treated at 50 μM with $\mathbf{16}^0$, $\mathbf{18}^-$, $\mathbf{42}^+$, and HpD and imaged using single-photon excitation, with a long-pass 505-nm emission filter; similar results were obtained with a long-pass 560-nm filter, the longest-wavelength filter available on the microscope. These filters pass the red pz emission but

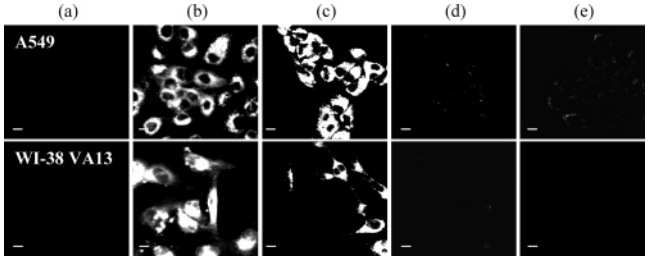

Figure 4. Cellular uptake of pzs using false-white single-photon confocal fluorescence microscopy images of A549 (top) and WI-38 VA13 (bottom) cells treated at 50 μM agent: (a) DMSO control, (b) HpD, (c) **16**^{0}, (d) **18**$^-$, (e) **42**$^+$. Scale bar = 10 μm.

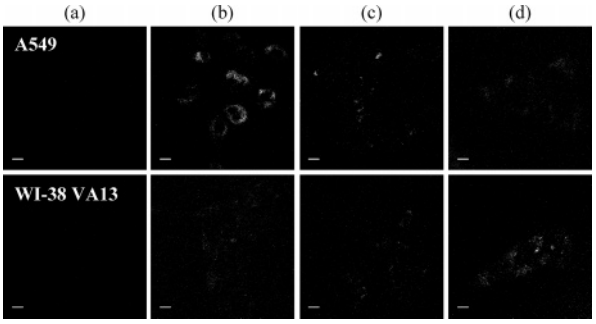

Figure 5. Cellular uptake of pzs using false-white two-photon confocal fluorescence microscopy images of A549 (top) and WI-38 VA13 (bottom) cells treated at 50 μM agent: (a) DMSO control, (b) **16**^{0}, (c) **18**$^-$, (d) **42**$^+$. Scale bar = 10 μm.

also the long-wavelength portion of the blue. To test the actual origin of the luminescence, images were collected with band-pass emission filters that exhaustively covered the range 500−717 nm. These measurements suggest that the blue fluorescence in fact provides a substantial component of the observed emission.

Pz **16**^{0} showed significant uptake and intracellular fluorescence, while pzs **18**$^-$ and **42**$^+$ exhibited little to no detectable intracellular fluorescence. The images indicate uniform staining of the cytoplasm by **16**^{0}, with no uptake by the nucleus; this interpretation is confirmed by images of successive planes within individual cells (not shown). The figure suggests that uptake of **16**^{0} is greater by the tumor A549 cells than the normal cells. Interestingly, although HpD is well-documented to be taken up better and held longer by tumor than by normal cells,[40,41] in these initial experiments there was no "washout" period, and HpD thus shows similar brightness in the two cell lines. Thus, it is potentially significant that **16**^{0} is incorporated better in the tumor cells in these experiments.

We explored the use of the dual-emission of the pzs, both the blue ($\lambda_{max} \sim 440$ nm) and red ($\lambda_{max} \sim 830$ nm) luminescence, in imaging pz uptake and localization. Because the microscope used had no excitation laser line at a sufficiently short wavelength to generate the blue pz fluorescence, we used two-photon excitation to monitor the UV luminescence.[42−44] Figure 5 compares the corresponding two-photon excitation confocal fluorescence images of tumor and normal cells treated for 24 h with 50 μM **16**^{0}, **18**$^-$, **42**$^+$; in this case, there is no HpD control because its emission profile ($\lambda_{max} \sim 615$ nm) is not compatible with this filter set. Although the images with this mode of detection are not as bright as the single-photon images of Figure 4, they show that in

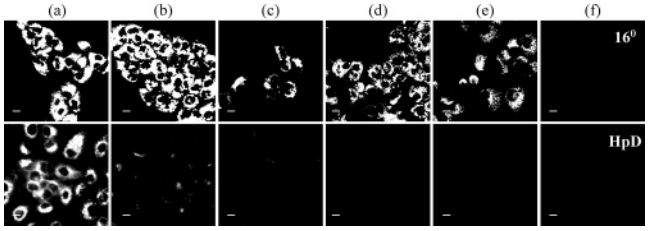

Figure 6. Concentration dependence of pz cellular uptake using false-white confocal fluorescence microscopy images of **16**^{0} (top) and HpD (bottom) in A549 cells. (a) 50 μM, (b) 25 μM, (c) 12.5 μM, (d) 6.2 μM, (e) 3.1 μM, (f) DMSO control. Scale bar = 10 μm.

fact all three pzs are taken up and fluoresce in both cell lines. As with the single-photon images, the most intense fluorescence is from **16**^{0}, and it again shows preferential incorporation into A549 cells. These images confirm that the pzs are distributed uniformly in the cytoplasm and are not taken up by the nucleus.

The bright fluorescence of pz **16**^{0} prompted a more careful comparison between it and HpD. Figure 6 shows that significant fluorescence (long-pass 505-nm emission filter) is detected from A549 treated with HpD at concentrations down to 25 μM. In contrast, fluorescence from incorporated pz **16**^{0} was visible under these conditions down to a treatment concentration of 3.1 μM, which is 8-fold lower.

The localization properties of **16**^{0} in A549 tumor cells were further examined through colocalization experiments with a known mitochondrial-specific dye, MitoTracker Green. With an absorbance maximum at 490 nm and emission maximum at 516 nm,[45] MitoTracker Green was used in conjunction with the blue emission of **16**^{0} to simultaneously test for colocalization of the two dyes. A higher concentration (100 μM) of **16**^{0} was employed in order to produce a more intense two-photon UV emission than that observed at 50 μM **16**^{0} (Figure 5); the higher concentration had no effect on cellular toxicity after the 24-h exposure period. Figure 7 (top row) shows individual fluorescence images of **16**^{0} (A, false-red fluorescence) and MitoTracker Green (B, false-green fluorescence) in A549 tumor cells, as well as the overlapped image (C) of the two dyes, where yellow areas represent regions of colocalization. Significant overlap of the two dyes is observed, suggesting that one of the primary intracellular targets of **16**^{0} is the mitochondria.

For comparison, LysoTracker Green, a lysosomal-specific dye having similar optical properties ($\lambda_{abs} = 504$ nm, $\lambda_{em} = 511$ nm) to those of MitoTracker Green, was also tested under the same conditions (Figure 7, bottom row). LysoTracker Green was found to exhibit only a very small amount of overlap with **16**^{0}, indicating that once incorporated into A549 cells, the neutral pz **16**^{0} interacts very little with the lysosomes.

It is noted that analogous colocalization studies of the normal cells could not be carried out because only faint fluorescence is observed upon two-photon excitation of **16**^{0} in WI-38 VA13 cells (Figure 5).

Quantitative in Vitro Effect of Porphyrazines. MTT proliferation/viability assays were performed for A549 and WI-38 VA13 cells grown in culture while exposed to compounds **16**^{0}, **18**$^-$, and **42**$^+$ at 50 μM over a time course of 72 h. The influence of the pzs on cell

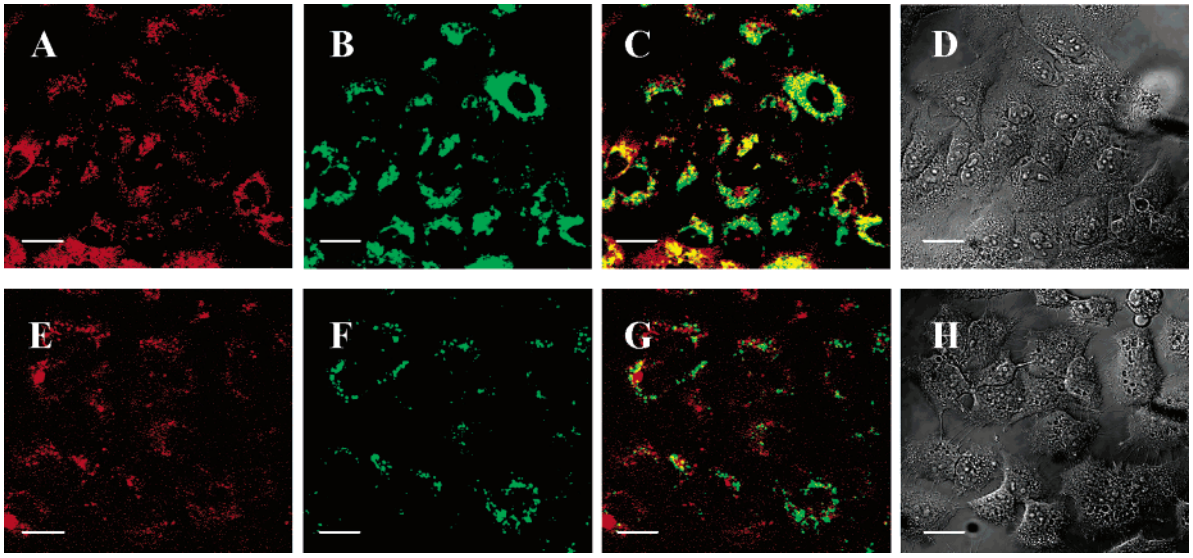

Figure 7. Intracellular colocalization of **16**^{0} and organelle-specific dyes in A549 cells: (top row) MitoTracker Green; (bottom row) LysoTracker Green; (A, E) false-red fluorescence of **16**^{0}; (B, F) false-green fluorescence of organelle-specific dye; (C, G) overlay, areas in yellow indicate co-localization; (D, H) phase contrast. Scale bar = 10 μm.

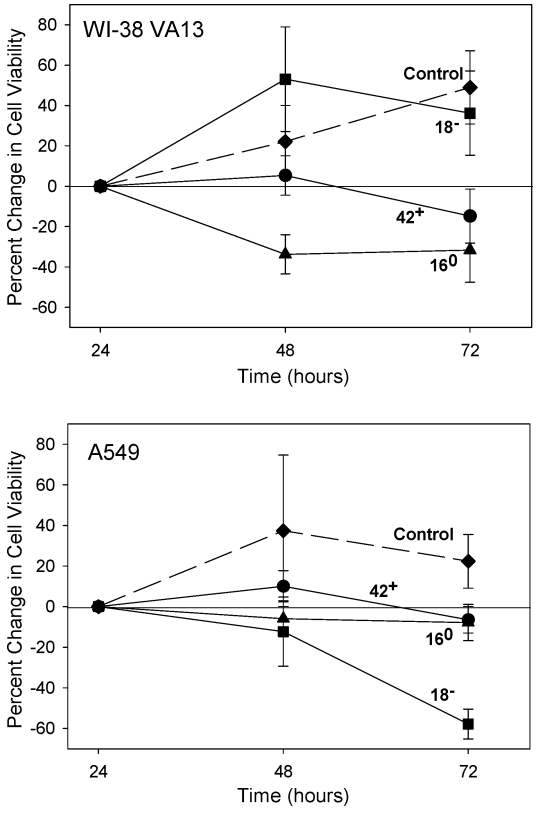

Figure 8. Cytotoxicity of **16**^{0}, **18**$^-$, and **42**$^+$, as measured by the MTT assay and reported as the percent change in cell viability between 24 and 72 h, upon exposure to 50 μM pz.

viability are minimal at 24 h; hence, Figure 8 presents the changes in cell viability between 24 and 72 h. Untreated cells show modest growth between 24 and 72 h. The positively charged pz **42**$^+$ weakly suppressed this growth for both cell lines, decreasing the viability at 72 h of the tumor cells by approximately 10% and the normal cells by about 20% (Figure 8). The neutral pz **16**^{0} behaved analogously, but reduced the viability of the normal WI-38 VA13 cells even more. Importantly, the behavior of **16**^{0} is *not* universal to neutral pzs of the class being studied here (Figure 2); for example,

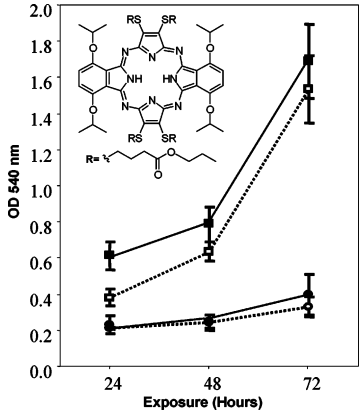

Figure 9. Cytotoxicity of **17**^{0} as measured by an MTT time course plot of A549 (□) and WI-38 VA13 (○) cells exposed to 50 μM **17**^{0}. Dotted lines, control (cells only); solid lines, cells + pz.

neither cell line showed any harmful effects upon treatment with **17**^{0} (Figure 9), the neutral tetra(propyl ester) precursor of **18**$^-$ (Scheme 1). The results for **16**^{0} and **17**^{0} suggest that the hydrophobicity of the R side chain represents an alternate "dimension" in which to vary the biological properties of a pz subclass.

The behavior of pz **18**$^-$ differs sharply from that of the other two. Treatment of A549 tumor cells with ~50 μM pz **18**$^-$ for 72 h causes progressive cell death that decreases the number of viable cells by 60−70% (Figure 8), while the same treatment of WI-38 VA13 normal cells with pz **18**$^-$ does not interfere with their growth. Thus, pz **18**$^-$ emerges as a candidate as an antitumor agent.

Dose-Dependent Effects of Pzs. To determine the dose dependence of the cellular response to pzs, the two cell lines were treated with compounds **16**^{0}, **18**$^-$, and **42**$^+$ at varying concentrations for 72 h. Figure 10 shows the percent cell viability of cells treated this way, calculated relative to the viability of untreated cells. As a control, both cell lines were similarly treated with 50 μM HpD, which caused no change from normal growth characteristics.

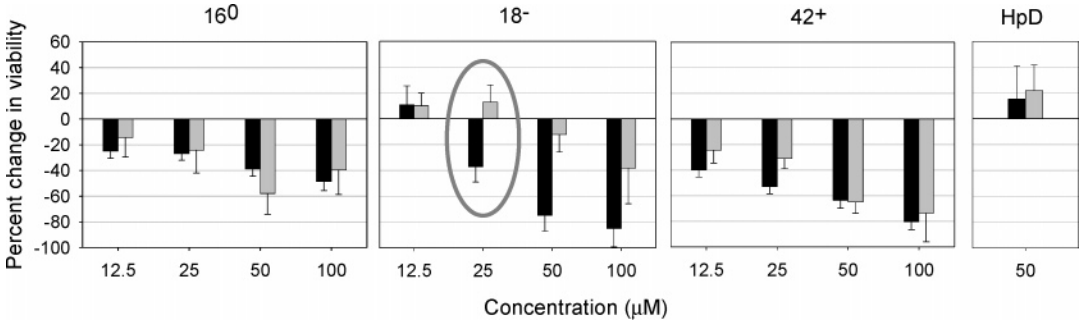

Figure 10. Dose-dependent cytotoxicity of pzs, as measured by the MTT assay and reported as the percent cell viability, relative to DMSO control, after 72-h exposure to pzs at 12.5, 25, 50, and 100 μM pz. Black bars, A549; gray bars, WI-38 VA13. The ellipse indicates a treatment concentration at which selective tumor toxicity is observed.

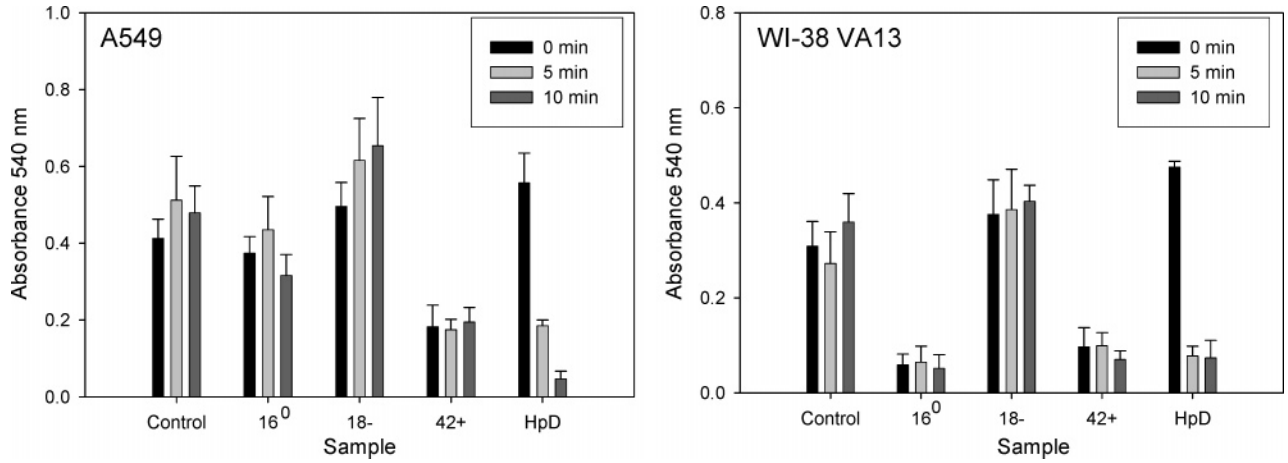

Figure 11. Phototoxicity effects of $\mathbf{16}^0$, $\mathbf{18}^-$, and $\mathbf{42}^+$, as measured by an MTT assay of A549 (left) and WI-38 VA13 (right) cells exposed to 50 μM pz or HpD for 24 h, followed by white light exposure for 0, 5, or 10 min.

The dose−response data of Figure 10 shows that pzs $\mathbf{16}^0$ and $\mathbf{42}^+$ are toxic to both A549 tumor and WI-38 VA13 normal cell lines over the concentration range studied (12.5−100 μM). The two pzs appear to differ slightly in that the response to $\mathbf{16}^0$ may be leveling at ~40% killing after 72 h of exposure to ~50 μM $\mathbf{16}^0$, whereas the dose−response curve of $\mathbf{42}^+$ is roughly linear, with about 70% cell killing of both tumor and normal cells after 72 h of exposure to 100 μM $\mathbf{42}^+$.

Most importantly, the dose−response measurements confirm that pz $\mathbf{18}^-$ differentially kills lung tumor cells. At the lowest treatment concentration of $\mathbf{18}^-$ used in this set of experiments, 12.5 μM, both cell types show modest growth, ~10% increase at 72 h. However, after 72 h exposure to 25 μM $\mathbf{18}^-$, the normal cells have grown equally well, whereas about 40% of the tumor cells have been killed.

The killing of the tumor cells by $\mathbf{18}^-$ is roughly linear with dose, increasing to over 80% with treatment of the pz at 100 μM. At the two higher concentrations of $\mathbf{18}^-$, it begins to show toxicity in the normal cells as well. The maximum difference between the two cell lines comes at 50 μM $\mathbf{18}^-$, where almost 80% of the tumor cells, but only about 10% of the normal cells, have been killed. The optimum difference would appear to occur with $\mathbf{18}^-$ at around 25 μM: 10% growth of normal cells after 72 h, about 40% inhibition of tumor cells. These findings suggest that $\mathbf{18}^-$ at this dose could be used to eventually kill all of the tumor cells, without harming normal cells.

Photosensitizing Effects of the Porphyrazines. The viability data presented above (Figures 8 and 10) describes the inherent toxicity of the pzs, without the additional light treatment used in PDT applications. To determine if light activation of these compounds in vitro resulted in additional toxicity through singlet oxygen generation, phototoxicity assays were carried out. Figure 11 shows toxicity data of cells exposed to no light versus those exposed to 5 and 10 min of white light exposure. Untreated cells were used as a control.

As expected, growth of the untreated cells was not adversely affected by the additional light exposure. Both cell lines demonstrated a significant light-dependent killing effect when exposed to HpD, as both A549 tumor and WI-38 VA13 normal cells were nearly completely killed upon 10 min light treatment in the presence of HpD. Conversely, the additional white light treatment showed little effect on any of the pzs studied in either cell line, as viability levels remained steady with and without light treatment.

Conclusions

We are preparing a large library of pzs for biological testing and here have reported the toxicity, cellular uptake, and localization in both tumor (A549) and normal (WI-38 VA13) cell lines of three members of the pz subclass depicted in Figure 2. Confocal fluorescence microscopy disclosed that the three pzs, which differ in charge, are all taken up by both cell lines. As best seen with $\mathbf{16}^0$, the pzs uniformly stain the cytoplasm, with

no uptake by the nucleus. The intracellular luminescence of $\mathbf{16}^0$ is more intense than that of the other two pzs, and the luminescence of $\mathbf{16}^0$ incorporated in the tumor cells is greater than that in the normal cells, which suggest that cellular uptake and differential tumor/normal uptake are charge dependent. The intracellular luminescence of $\mathbf{16}^0$ was visible at treatment concentrations as low as 3.1 μM; for comparison, the clinically approved porphyrin compound, Photofrin (HpD), has poor photophysical properties and its fluorescence was undetectable at concentrations of 12.5 μM and below. Colocalization tests with a mitochondrial-specific dye suggest that $\mathbf{16}^0$ localizes in the mitochondria of A549 tumor cells.

Although the optical properties of this class of pzs make them attractive as optical imaging/antitumor agents, MTT cytotoxicity assays disclose that $\mathbf{16}^0$ and $\mathbf{42}^+$ are not likely potential biomedical agents, as they are less harmful to tumor than to normal cells. Experiments in progress with other pzs have disclosed compounds benign to both tumor and normal cells, as well as other pzs with selective tumor toxicity. Intriguingly, the assays presented here suggest that $\mathbf{18}^-$ offers promise as a traditional antitumor agent: it preferentially kills lung adenocarcinoma cells, and at a treatment concentration of 25 μM, it is harmless to the normal WI-38 VA13 cells over 72 h, while killing about 40% of the A549 tumor cells.

Unlike traditional photodynamic therapy photosensitizers, the toxicity effects observed in the MTT assays of $\mathbf{16}^0$, $\mathbf{18}^-$, and $\mathbf{42}^+$ are independent of illumination with light. A slight intracellular aggregation may persist for these compounds in aqueous environments, thereby suppressing singlet oxygen generation, an effect that has been seen in other porphyrinic systems.[46] The free-base pzs have inherently lower singlet oxygen quantum yields than their metalated counterparts. Both the solubilities in aqueous medium and quantum yields are enhanced in analogous M = Mg or Zn pzs;[32] thus, future experiments will probe the effect of various M on the biological behavior of the pzs. Additional tumor cell types will be examined to determine the universality of $\mathbf{18}^-$ as an antitumor agent, and uptake/release measurements in progress will explore the evidence for selective uptake of this pz by tumor cells. On the basis of the initial biological findings reported here, however, it seems safe to suggest that the pzs as a class offer substantial promise as biomedical agents.

Acknowledgment. The authors would like to thank Dr. Nina Brown, Mrs. Janet Wolford, and Mrs. Anja Herrnreiter for many helpful discussions and help with the two-photon experiments. This work was supported by the NIH (CA 88850) and a VA Merit Review Grant.

Supporting Information Available: ^{1}H NMR for compounds **1**, $\mathbf{15}^0$, $\mathbf{16}^0$, $\mathbf{17}^0$, and $\mathbf{18}^-$ and elemental analysis data for compound $\mathbf{42}^+$. This material is available free of charge via the Internet at http://pubs.acs.org.

References

(1) Kessel, D.; Dougherty, T. J. Agents Used in Photodynamic Therapy. *Rev. Contemp. Pharmacother.* **1999**, *10*, 19−24.
(2) Dolmans, D. E. J. G. J.; Fukumura, D.; Jain, R. K. Photodynamic Therapy for Cancer. *Nat. Rev. Cancer* **2003**, *3*, 380−387.
(3) Bonnett, R. Photosensitizers of the Porphyrin and Phthalocyanine Series for Photodynamic Therapy. *Chem. Soc. Rev.* **1995**, 19−33.
(4) Pandey, R. K.; Zheng, G. Porphyrins as Photosensitizers in Photodynamic Therapy. In *The Porphyrin* Handbook; Kadish, K. M., Smith, K. M., Guilard, R., Eds.; Academic Press: New York, 2000; Vol. 6, pp 157−227.
(5) Jiang, H.; Iftimia N. V.; Xu, Y.; Eggert J. A.; Fajardo L. L.; Klove K. L. Near-Infrared Optical Imaging of the Breast with Model-Based Reconstruction. *Acad. Radiol.* **2002**, *9*, 186−194.
(6) Weissleder, R.; Ntziachristos, V. Shedding Light onto Live Molecular Targets. *Nat. Med.* **2003**, *9*, 123−128.
(7) Sevick-Muraca, E. M.; Godavarty, A.; Houston, J. P.; Thompson, A. B.; Roy, R. Near-Infrared Imaging with Fluorescent Contrast Agents. In *Fluorescence in Biomedicine*; Pogue, B. W., Mycek, M., Eds.; Marcel Dekker: New York, 2003; pp 445−527.
(8) Chance, B.; Alfano, R. R.; Tromberg, B. J.; Tamura, M.; Sevick-Muraca, E. M.; Eds. *Proceedings of the SPIE International Conference on Optical Tomography and Spectroscopy of Tissue V;* January 26−29, 2003, San Jose, CA [In *Proc. SPIE-Int. Soc. Opt. Eng.* **2003**, 4955].
(9) Quaresima, V.; Matcher, S. J.; Ferrari, M. Identification and Quantification of Intrinsic Optical Contrast for Near-Infrared Mammography. *Photochem. Photobiol.* **1998**, *67*, 4−14.
(10) Troy, T. L.; Page, D. L.; Sevick-Muraca, E. M. Optical Properties of Normal and Diseased Breast Tissues: Prognosis for Optical Mammography. *J. Biomed. Opt.* **1996**, *1*, 342−355.
(11) de Haller, E. B. Time-Resolved Transillumination and Optical Tomography. *J. Biomed. Opt.* **1996**, *1*, 7−17.
(12) MacDonald, I. J.; Dougherty, T. J. Basic Principles of Photodynamic Therapy. *J. Porphyrins Phthalocyanines* **2001**, *5*, 105−129.
(13) Allen, C. M.; Sharman, W. M.; Van Lier, J. E. Current Status of Phthalocyanines in the Photodynamic Therapy of Cancer. *J. Porphyrins Phthalocyanines* **2001**, *5*, 161−169.
(14) Liu, W.; Jensen, T. J.; Fronczek, F. R.; Hammer, R. P.; Smith, K. M.; Vicente, M. G. H. Synthesis and Cellular Studies of Nonaggregated Water-Soluble Phthalocyanines. *J. Med. Chem.* **2005**, *48*, 1033−1048.
(15) Chowdhary, R. K.; Shariff, I.; Dolphin, D. Drug Release Characteristics of Lipid Based Benzoporphyrin Derivative. *J. Pharm. Pharm. Sci.* **2003**, *6*, 13−19.
(16) Pandey, R. K. Synthetic strategies in designing porphyrin-based photosensitizers for photodynamic therapy. In *CRC Handbook of Organic Photochemistry and Photobiology*, 2nd ed.; Horspool, W., Lenci, F., Eds.; CRC Press: Boca Raton, FL, 2004; pp 144-1−144-21.
(17) Sessler, J. L.; Seidel, D. Synthetic Expanded Porphyrin Chemistry. *Angew. Chem., Int. Ed.* **2003**, *42*, 5134−5175.
(18) Michel, S. L. J.; Baum, S.; Barrett, A. G. M.; Hoffman, B. M. Peripherally Functionalized Porphyrazines: Novel Metallomacrocycles with Broad, Untapped Potential. *Prog. Inorg. Chem.* **2001**, *50*, 473−590.
(19) Cook, A. S.; Williams, D. B. G.; White, A. J. P.; Williams, D. J.; Lange, S. J.; Barrett, A. G. M.; Hoffman, B. M. Enantiomerically Pure "Winged" Spirane Porphyrazinoctaols. *Angew. Chem., Int. Ed. Engl.* **1997**, *36*, 760−761.
(20) Sibert, J. W.; Baumann, T. F.; Williams, D. J.; White, A. J. P.; Barrett, A. G. M.; Hoffman, B. M. Gemini Porphyrazines: The Synthesis and Characterization of Metal-Capped cis- and *trans*-Porphyrazine Tetrathiolates. *J. Am. Chem. Soc.* **1996**, *118*, 10487−10493.
(21) Lange, S. J.; Nie, H.; Stern, C. L.; Barrett, A. G. M.; Hoffman, B. M. Peripheral Palladium(II) and Platinum(II) Complexes of Bis(dimethylamino)porphyrazine. *Inorg. Chem.* **1998**, *37*, 6435−6443.
(22) Forsyth, T. P.; Williams, D. B. G.; Montalban, A. G.; Stern, C. L.; Barrett, A. G. M.; Hoffman, B. M. A Facile and Regioselective Synthesis of Trans-Heterofunctionalized Porphyrazine Derivatives. *J. Org. Chem.* **1998**, *63*, 331−336.
(23) Linben, T. G.; Hanack, M. Synthesis, Separation and Characterization of Unsymmetrically Substituted Phthalocyanines. *Chem. Ber.* **1994**, *127*, 2051−2057.
(24) Kobayashi, N.; Ashida, T.; Osa, T. Synthesis, Spectroscopy, Electrochemistry, and Spectroelectrochemistry of a Zinc Phthalocyanine with D_{2h} Symmetry. *Chem. Lett.* **1992**, 2031−2034.
(25) Stihler, P.; Hauschel, B.; Hanack, M. Synthesis of a Bisdienophilic Phthalocyanine and of Precursors for Repetitive Diels−Alder Reactions Based on Hemiporphyrazines and Phthalocyanines. *Chem. Ber.* **1997**, *130*, 801−806.
(26) Leznoff, C. C.; Svirskaya, P. I.; Khouw, B.; Cerny, R. L.; Seymour, P.; Lever, A. B. P. Syntheses of Monometalated and Unsymmetrically Substituted Binuclear Phthalocyanines and a Pentanuclear Phthalocyanine by Solution and Polymer Support Methods. *J. Org. Chem.* **1991**, *56*, 82−90.
(27) Lee, S.; Stackow, R.; Foote, C. S.; Barrett, A. G. M.; Hoffman, B. M. Tuning the Singlet Oxygen Quantum Yield of Near-IR-Absorbing Porphyrazines. *Photochem. Photobiol.* **2003**, *77*, 18−21.
(28) Carvalho, V. C. M.; Melo, C. A. S.; Bagnato, V. S.; Perussi, J. R. Comparison of the Effects of Cationic and Anionic Porphyrins in Tumor Cells Under Illumination of Argon Ion Laser. *Laser Phys.* **2002**, *12*, 1314−1319.

(29) Ruck, A.; Kollner, T.; Dietrich, A.; Strauss, W.; Schneckenburger, H. Fluorescence Formation During Photodynamic Therapy in the Nucleus of Cells Incubated with Cationic and Anionic Water-Soluble Photosensitizers. *J. Photochem. Photobiol., B: Biol.* **1992**, *12*, 403−412.
(30) Juarranz, A.; Villanueva, A.; Diaz, V.; Canete, M. Photodynamic Effects of the Cationic Porphyrin, Mesotetra(4*N*-methylpyridyl)-porphyine, on Microtubules of HeLa Cells. *J. Photochem. Photobiol., B: Biol*. **1995**, *27*, 47−53.
(31) Ehrlich, L. A.; Skrdla, P. J.; Jarrell, W.; Sibert, J. W.; Armstrong, N. R.; Saavedra, S. S.; Barrett, A. G. M.; Hoffman, B. M. Preparation of Polyetherol-Appended Sulfur Porphyrazines and Investigations of Peripheral Metal Ion Binding in Polar Solutions. *Inorg. Chem.* **2000**, *39*, 3963−3969.
(32) Lee, S.; White, A. J. P.; Williams, D. J.; Barrett, A. G. M.; Hoffman, B. M. Synthesis of Near-IR Absorbing/Emitting Porphyrazine Derivatives with Tunable Solubility. *J. Org. Chem.* **2001**, *66*, 461−465.
(33) Davison, A.; Holm, R. H. Metal Complexes Derived from *cis*-1,2-dicyano-1,2-ethylenedithiolate and Bis(trifluoromethyl)-1,2-dithiete. *Inorg. Synth.* **1967**, *10*, 8−26.
(34) The HpD concentration was calculated using an assigned molecular weight of 600.
(35) Giard, D. J.; Aaronson, S. A.; Todaro, G. J.; Arnstein, P.; Kersey, J. H.; Dosik, H.; Parks, W. P. In Vitro Cultivation of Human Tumors: Establishment of Cell Lines Derived from a Series of Solid Tumors. *J. Natl. Cancer Inst.* **1973**, *51*, 1417−1423.
(36) Lieber, M.; Smith, B.; Szakal, A.; Nelson-Rees, W.; Todaro, G. A Continuous Tumor-Cell Line from a Human Lung Carcinoma with Properties of Type II Alveolar Epithelial Cells. *Int. J. Cancer.* **1976**, *17*, 62−70.
(37) Girardi, A. J.; Weinstein, D.; Moorhead, P. S. SV40 Transformation of Human Diploid Cells. A Parallel Study of Viral and Karyologic Parameters. *Ann. Med. Exp. Biol. Fenn.* **1966**, *44*, 242−254.
(38) Hayflick, L.; Moorhead, P. S. The Serial Cultivation of Human Diploid Cell Strains. *Exp. Cell Res.* **1961**, *25*, 585−621.
(39) Hayflick, L. The Limited in Vitro Lifetime of Human Diploid Cell Strains. *Exp. Cell Res.* **1965**, *37*, 614−636.
(40) Dougherty, T. J. Photodynamic Therapy (PDT) of Malignant-Tumors. *Crit. Rev. Oncol. Hematol.* **1984**, *2*, 83−116.
(41) Little, F. M.; Gomer, C. J.; Hyman, S.; Apuzzo, M. L. J. Observations in Studies of Quantitative Kinetics of Tritium Labeled Hematoporphyrin Derivatives (HpDI and HpDII) in the Normal and Neoplastic Rat Brain Model. *J. Neuro-Oncol.* **1984**, *2*, 361−370.
(42) Williams, R. M.; Zipfel, W. R.; Webb, W. W. Multiphoton Microscopy in Biological Research. *Curr. Opin. Chem. Biol.* **2001**, *5*, 603−608.
(43) So, P. T. C.; Dong, C. Y.; Masters, B. R.; Berland, K. M. Two-Photon Excitation Fluorescence Microscopy. *Annu. Rev. Biomed. Eng.* **2000**, *2*, 399−429.
(44) Denk, W.; Piston, D. W.; Webb, W. W. Two-Photon Molecular Excitation in Laser-Scanning Microscopy. In *Handbook of Biological Confocal Microscopy*; Pawley, J. B., Ed.; Plenum Press: New York, 1995; pp 445−458.
(45) Haugland, R. P. Chapter 12: Probes for Organelles. In *Handbook of Fluorescent Probes and Research Products*, 9th ed.; Haugland, R. P., Spence, M. T. Z.; Johnson, I. D., Gregory, J., Eds.; Molecular Probes: Eugene, OR, 2002; pp 469−502.
(46) Tanielian, C.; Schweitzer, C.; Mechin, R.; Wolff, C. Quantum Yield of Singlet Oxygen Production by Monomeric and Aggregated Forms of Hematoporphyrin Derivative. *Free Radical Biol. Med.* **2001**, *30*, 208−212.

JM050466Y